

Observational Evidence of Sausage-Pinch Instability in Solar Corona by SDO/AIA

A.K. Srivastava¹

¹*Aryabhata Research Institute of Observational Sciences (ARIES), Manora Peak, Nainital-263 129, India*

R. Erdélyi²

²*Solar Physics and Space Plasma Research Centre (SP2RC), School of Mathematics and Statistics, The University of Sheffield, Sheffield, U.K.*

Durgesh Tripathi³

³*Inter-University Centre for Astronomy and Astrophysics, Post Bag 4, Ganeshkhind, Pune 411007, India.*

V. Fedun^{2,4}

²*Solar Physics and Space Plasma Research Centre (SP2RC), School of Mathematics and Statistics, The University of Sheffield, Sheffield, U.K.*

⁴*Department of Automatic Control and Systems Engineering, The University of Sheffield, Mappin Street, Sheffield S1 3JD, U.K.*

N.C. Joshi¹, P. Kayshap¹

Aryabhata Research Institute of Observational Sciences (ARIES), Manora Peak, Nainital-263 129, India.

ABSTRACT

We present the first observational evidence of the evolution of sausage-pinch instability in Active Region 11295 during a prominence eruption using data recorded on 12 September 2011 by the Atmospheric Imaging Assembly (AIA) onboard the Solar Dynamics Observatory (SDO). We have identified a magnetic flux tube visible in AIA 304 Å that shows curvatures on its surface with variable cross-sections as well as enhanced brightness. These curvatures evolved and thereafter smoothed out within a time-scale of a minute. The curved locations on the flux tube exhibit a radial outward enhancement of the surface of about 1-2 Mm (factor of 2 larger than the original thickness of the flux tube) from the equilibrium position. AIA 193 Å snapshots also show the formation of bright knots and narrow regions inbetween at the four locations as that of 304 Å along the flux tube where plasma emission is larger compared to the background. The formation of bright knots over an entire flux tube as well as the narrow regions in < 60 s may be the morphological signature of the sausage instability. We also find the flows of the confined plasma in these bright knots along the field lines, which indicates the dynamicity of the flux tube that probably causes the dominance of the longitudinal field component over short temporal scales. The observed longitudinal motion of the plasma frozen in the magnetic field lines further vanishes the formed curvatures and plasma confinements as well as growth of instability to stabilize the flux tube.

Subject headings: Sun: corona – magnetohydrodynamics (MHD) – magnetic reconnection – Sun: flares

1. Introduction

A wide range of MHD instabilities have been observed in solar atmosphere in recent years in association with various dynamical processes (e.g. Williams et al. 2005; Srivastava et al. 2010; Foullon et al. 2011, and references therein). Kumar et al. (2010) discovered evidence of coalescence instability for loop-loop interaction in association with M7.9/1N class solar flare as previously theoretically investigated in great details (e.g. Tajima et al. 1982; Sakai & de Jager 1996). Kliem et al. (2000) have also reported the dynamical reconnection scenario by repeated formation and subsequent coalescence of magnetic islands in solar active regions. Recently, Innes et al. (2012) interpreted the break-up and finger like structures in down-flowing plasma following a filament eruption on 7 June 2011 as evidence of Rayleigh-Taylor instability. Hillier et al. (2012) and Hillier et al. (2012) have numerically modelled Rayleigh-Taylor instability in the solar prominences to explain the observed plasma upflows and reconnection triggered downflows. Ballooning and torus instabilities have also been reported as one of the prominent mechanisms for flux rope eruptions (Aulanier et al. 2010). Tsap et al. (2008) have reported the generation of ballooning instability due to the confined kink instability in ideal MHD regime applicable to the solar atmosphere as previously analytically modelled by, e.g., Hood & Priest (1979). Furthermore, Kelvin-Helmholtz and Alfvén instabilities in the solar corona are also observed and theorized by various authors (Foullon et al. 2011; Ofman & Thompson 2011; Taroyan 2011). Motivated by the observations of these instabilities using here excellent high-resolution data from the Transition Region and Coronal Explorer (TRACE), Hinode and SDO missions, a considerable effort has gone into analytical and numerical modelling in order to study the characteristics of the different types of instabilities (see e.g. Török et al. 2004; Török & Kliem 2005; Haynes & Arber 2007; Taroyan 2011; Soler et al. 2010; Zaqarashvili et al. 2010; Botha et al. 2012, and references cited therein).

The kink-unstable mode ($m=1$) of cylindrical magnetic flux tubes may seem to be observed frequently in the solar corona (Srivastava et al.

2010). However, another type of instability known as sausage instability ($m=0$) mode, which is theoretically investigated in astrophysical plasma (Priest 1982; Sturrock 1994; Aschwanden 2004), to the best of our knowledge, has not yet been observed in solar atmosphere. In a cylindrical magnetic flux tube, the inward directed Lorentz force is counteracted by increasing the gas plasma pressure gradient that is directed outward, and evolution of such instability takes place after meeting certain criteria, i.e., $B_\theta/B_z > 1.4$ (see Kadomtsev 1966; Aschwanden 2004). In the present paper, we outline the observational evidence of sausage pinch instability evolving in an eruptive flux tube from the Active Region NOAA AR 11295 on 12 September 2011. In section 2 we describe the observations. In section 3 we report the detection of sausage-pinch instability in corona. The last section contains the summary and discussions.

2. Observations

A C9.9 class solar flare was observed during the emergence of active region AR11295 (N21E59) at the North-East limb on 12 September 2011. The flare started at 20:30 UT with peak intensity at 20:54 UT, and ended at 21:51 UT. We have used imaging data showing the dynamics of AR 11295 as observed by the SDO/AIA, which has a maximum resolution of 0.6" per pixel and a cadence of 12 s. AIA provides full disk observations of the Sun in three ultra-violet (UV) continua at 1600 Å, 1700 Å, 4500 Å, and seven Extreme Ultra-Violet (EUV) narrow bands at 171 Å, 193 Å, 211 Å, 94 Å, 304 Å, 335 Å, and 131 Å respectively (Lemen et al. 2012). Therefore, it provides observations of multi-temperature, high spatial and temporal resolution plasma dynamics of solar atmosphere. Here, we use the data recorded by two filters of AIA, namely, 304 Å and 193 Å. The images recoded in 304 Å (max. formation temperature $T_f=10^5$ K) provides information about the plasma dynamics in upper chromosphere and lower transition region, whereas those in 193 Å ($T_f=1.58 \times 10^6$ K) reveal information about the lower corona. The primary contributing ion and the temperature response for each of these channels can vary, depending on the plasma features on the Sun's surface being observed (O'Dwyer et al. 2011; Del Zanna et al. 2011). The time-series of SDO/AIA data has been reduced by the SSW

cutout service ¹.

3. Detection of Sausage-pinch Instability

Fig. 1 shows the images of the active region AR 11295 and the regions in their vicinity at the North-East limb recorded using 304 Å (left panel) and 193 Å filters (right panel). Two filament channels are visible in these snapshots highlighted by green and yellow arrows. The eastward filament channel marked by yellow arrow becomes partially activated around 20:45 UT, well before the start of the flare. The filament passes through different topological changes and shows plasma heating before it finally kinks and erupts partially (cf., MFT.mpeg). This eruption is classified as partial eruption (e.g. Gilbert et al. 2000; Gibson & Fan 2006; Tripathi et al. 2007, 2009, 2013).

In Fig. 2, the left and right vertical columns, respectively, show the time-series of the partial and zoomed FOV of a rising flux tube (part of the erupting prominence) in AR 11295 for a rather short duration of 20:47-20:48 UT in 304 Å and 193 Å. During this period, we note that, the flux tube does not rise much as is evident from Fig. 2 despite there are considerable topological changes as well as plasma flows. The top row in Fig. 2 demonstrates the internal reconnection above the two footpoints of the flux tube and energy release via kinking. The southern foot-point of the flux tube becomes disconnected during the evolutionary process due to reconnection, and its connectivity is changed. This facilitates the slow rise of the flux tube in the corona.

The twist is transferred in the remaining part of the magneto-plasma of the flux tube. It should also be noted that the enveloping closed flux tube is overlying the complex magnetic field configuration and associated plasma in the core of the active region. The flux tube reveals concave and non-static curvatures at various locations on surface (cf., 304 Å snapshot in the second row) on both side. We have marked these locations by green (northern side) and blue (southern side) arrows. The concave curvatures appear like bright knots due to the enhance emission at those locii. This could be explained in terms of line-of-sight (LOS) integration of the emission. It is also observed

that the narrow regions also become brighter along with knots. This may be due to the highly dynamic nature of flux tube and its plasma that is flowing along with field lines (cf., Fig. 5). Apart from sub-mega Kelvin (304 Å) and mega-Kelvin (193 Å) AIA channels, we also examined a more hotter flare channel of 131 Å in which co-temporal data is available. The appearance of the same enhanced areas, as visible in 304 Å in Fig. 2, are also evident in this particular band in the enveloping flux tube. The flare energy is enhanced in the low-lying southward directed loop systems (not shown here) in the same active region, although, it is not directly related with the observed flux tube. The plasma may be multi-thermal leading us to see that in the multi-channels of AIA. However, the extent to which this emission is seen in multiple co-temporal channels is almost the same. Therefore, it is plausible to conclude that these bright knots are not due to heating effects.

At the locii where the cross-section of the flux tube has increased more plasma may be accommodated. While, other locii where the flux tube is 'pinched' and has smaller cross-sections may have rarefaction and less plasma density (Syrovatskii 1981). Since the radiation in the corona is essentially optically thin, the locii with enhanced cross-sections appear brighter. This phenomenon can also be seen in the 193 Å (second row, right panel) image and is shown by the arrows. From the images in the third row, this is further evident in both wavelengths that the increased cross-sections in form of knots are more evolved (cf., 20:47:55 UT snapshots). The phenomenon is well observed in some particular AIA channels in which the LOS contribution of the plasma is significant in filling these regions of the flux tube. Moreover, this is very short duration dynamics observed by few AIA channels successfully and co-temporally. We note here that these curvatures faded away within ~ 1.0 minutes of their evolution from the entire body of the flux tube. The plasma necks (refer to narrow regions in the current resolution of AIA) are formed in-between these knots, which are the pinched regions. However, the exact quantification of flux tube necks, i.e., decrease in loop width opposite to the sausage knots, is not plausible in the observed thin and enveloping flux tube of radius 1 Mm considering the current resolution of AIA (0.6"/pixel).

¹http://lmsal.com/get_aia_data/

We interpret these observations as the most likely evolution of sausage-pinch instability in the early phase of partially eruptive flux tube in NOAA AR11295. The flux tube becomes unstable at the knot locations (cf., schematics overlaid on AIA snapshots in Fig. 3) where the confining field is most likely concave and the longitudinal field is less dominant over the local azimuthal component. This leads to an instability known as the sausage pinch instability. The Lorentz force, and therefore the pinch-instability in a plasma cylinder, could be generated either by an axial current or by presence of an ambient longitudinal magnetic field. In the first situation, in the plane which is perpendicular to the axis, the internal current j_z generates an azimuthal magnetic field B_θ around itself. Interaction of the axial current with the induced magnetic field leads to excitation of the z -pinch instability of the plasma cylinder (cf., Fig. 3, top-left panel). On the other hand, the longitudinal magnetic field inside the flux tube when varies along its radius at a particular height, then induces an azimuthal current (j_θ). During interaction of this current with the ambient magnetic field, an inwardly directed Lorentz force is generated that confine the plasma in cylindrical geometry. This effect is known as θ -pinch instability (cf., Fig. 3, top-right panel). At the locii where the plasma column is pinched it can be stabilized against the sausage z -pinch instability by a longitudinal field that is significantly dominant over the azimuthal component (for more details see Kadomtsev 1966; Aschwanden 2004). The θ -pinch is neutrally stable and, therefore, stability also depends on additional ambient fields (see e.g. Freidberg 1982). Either mechanism may enforce the sausage instability at a particular moment in the flux tube. However, it should be noted that the present observational base-line can not distinguish between these two mechanisms and it should be considered as general interpretation of the instability.

The Time-Distance maps (Fig. 4) also reveal the dynamics of the increased cross-sectional areas over the fluxtube between the narrow pinched and straight regions. For example, the time-distance diagrams in AIA 304 Å along the slits are drawn across the various surface curvatures over the flux tube marked by position 'A', 'B' on its southward part, and 'D' on northward part as shown

in SDO/AIA 193 and 304 Å snapshots at 20:47 UT (cf., Fig. 2). The initial positions of the vertical slits (top-right corners in each Time-Distance diagram) are taken at the central core of the active region to which the fluxtube is enveloping. This point is considered as reference point, and all distances along the slit are measured w.r.t. this position. In time, the variation in the surface curvatures (ripples) and their evolution are clearly shown in Fig. 4. The top-left panel of Fig. 4 shows the time-distance plot along the slit placed across curvature 'A' (cf., Fig. 2). The surface of the flux tube rises vertically up to ~ 1.0 Mm outward and then, again, subsided back. Similarly, the curvatures at positions 'B', and 'D' (cf., top-right and bottom-left panels in Fig. 4), respectively, show the outward displacements of ~ 1.5 Mm, ~ 2 Mm, in the projection that subsided within 1.0 min. We exclude the measurement on the knot marked as 'C' in Fig. 2 as this portion outgrows obliquely and we may not have true variations in its outer surface curvature. We notice qualitative signature of the formation of bright knot at this position. The last panel of Fig. 4 shows almost no variation of the surface of clearly evolved neck between knots B and C. This region is not associated with any sliding motion of plasma blobs, e.g., as observed between A & B and C & D. A small pinching is also evident that recovers in time in dynamic flux tube. In this dynamic flux tube, it is difficult to constrain purely static pinched regions. However, this measurement shows that such regions may be created for some definite duration. Therefore, non-ideally though under the regime of dynamic flux tube, the morphological evidence of sausage-pinch instability incurred.

Kruskal-Shafranov condition for a tube of half length 'L' and half-width 'a' that subjects to the internal kink instability (m=1) mode is

$$2L > \lambda_s = \frac{2\pi a B_z}{B_\theta}. \quad (1)$$

Using the loop morphological parameters (L \sim 36 Mm, a \sim 1 Mm) and equation, we get $B_\theta/B_z > 2\pi a/2L \approx 0.08$. This means that if the conditions for sausage-pinch instability (m=0) is met (i.e., $B_\theta/B_z > 1.4$), the tube is already subjected to the kink instability. The bottom-left panel of Fig. 3 also shows the formation of kinked flux tube and internal magnetic reconnection. The initial kink instability

later most likely triggers the formation of sausage knots as well as counteracted pinched regions. The possible physical mechanisms underlying of these observations are illustrated in Fig. 3.

4. Results and Discussion

In this paper we present observational evidences of the evolution of bright knots and narrow region in between , as well as cross-sectional variation at **these** places over a flux tube in AR11295. These variations are seen on a rather short time scale of 1.0 min. The radial outward displacements of the concave surfaces of the observed flux tube are found to lie within the range of 1-2 Mm. Our observations show that the places with increased cross-sections are almost double at a time of the normal width of flux tube. This is a morphological evidence for the evolution of sausage-pinch instability. The activation of sausage-pinch instability attempts to disrupt the confined plasma of the flux tube in lateral direction, while the pinched regions work oppositely and force the plasma along field lines in the longitudinal direction.

We conjecture that pinched regions of the observed flux tube in-between the sausage-unstable parts are evident as more field-aligned and straighter where the longitudinal magnetic field (B_z) seems to be dominant over the azimuthal component (B_θ). These are the 'neck' parts of flux tube in-between the 'bulky blobs' of sausage-unstable parts (cf., 193 Å snapshot on 20:47:56 UT), which is the typical morphological scenario of a sausage-pinch unstable flux tube. This is suggestive of the fact that the longitudinal component of the magnetic field in the pinched regions becomes dominant.

Since the flux tube is changing its geometry and connectivity during eruption, therefore, the local active region dynamics and magnetoplasma configuration may not allow the full growth of sausage-pinch instability in the flux tube that depends highly on its morphology as well as plasma properties (Aschwanden 2004). The observed thin flux tube initially seems to be enveloping the various other dynamic flux tubes lying below and above of it. It should be noted that it is not a static flux tube where plasma confinement may occur in the form of static sausage and pinched regions. It was the part of the bulk flux-rope sys-

tem, which was very complex and dynamic, and containing many flux tubes interacting and reconnecting with each other especially in the core. This is the reason that bulk field-aligned longitudinal plasma motion (propagation of brightness) is evident in the flux tube (cf., Fig. 5). The plasma at the locations 'A', 'B' of sausage-brightened knots moves with speeds of 113 km s^{-1} , and 125 km s^{-1} . While, the curvature on 'D' first appeared and thereafter shrinks and slides in northward direction along the flux tube with speed of 170 km s^{-1} . Therefore, this may be the indication of the dominant longitudinal field and aligned plasma motions in the flux tube system locally, which vanishes further the creation of static magnetic islands and confinement of the plasma under the regime of sausage-pinch instability.

Some other alternative mechanisms may also play role in the formation of the observed bright plasma knots. Initially, the kinked flux tube may undergo in an internal reconnection and energy release. This The bursty reconnection due to the initial kink instability may also cause the formation of bright knots that could be the "magnetic islands" formed by internal reconnection (Kliem et al. 2000). The formation of such magnetic islands in resistive corona is reported to occur quasi-periodically at comparatively larger spatio-temporal scales under the scenario of recurrent and dynamic reconnection in the current sheet (Kliem et al. 2000). Such mechanism, may play some role, however, the direct comparison is not possible in the present observational baseline as it deals the short spatio-temporal dynamics and do not have a signature of periodic occurrence of reconnection and the associated formation of the magnetic islands due to tearing mode instabilities. The ballooning instability can also create plasma magnetic islands near the loop apex due to the difference in plasma beta at its upper boundary as well as below maintained layers (Shibasaki 1999; Tsap et al. 2008). Our observed morphological scenario of the formation of multiple bright knots (ripples) over the whole body of the flux tube for $<60 \text{ s}$ is entirely different from the evolution of the ballooning instability as observed recently (Kumar et al. 2012).

In conclusion, our observations provide the evidence of morphological evolution of sausage-pinch instability in the corona. Further observations

are required to fully understand its behaviour in corona. These observations may have implications to forthcoming theoretical and observational studies in understanding the role of such rare instability processes. More analysis should be performed in this direction using future high-resolution ground- and space based observations, which will provide new clues to the existing theories of sausage-pinch instability in magnetic flux tubes.

5. Acknowledgments

We thank referee for the constructive suggestions received that improved the paper. We acknowledge the use of the SDO/AIA observations for this study. RE acknowledges M. Kéry for patient encouragement and is also grateful to NSF, Hungary (OTKA, Ref. No. K83133) for financial support received. AKS also thanks Shobhna Srivastava for her support and encouragement. VF thanks Dr D. Vasylyev for his help with images preparation. DT acknowledge the support from DST under Fast Track Scheme (SERB/F/3369/2012-2013). AKS highly acknowledges the adoption of the method of E. Verwichte in making the Time-Distance diagrams along the curved paths.

REFERENCES

- Aschwanden, M. J. 2004, *Physics of the Solar Corona*,
- Aschwanden, M. J. 2009, *Space Sci. Rev.*, 149, 31
- Aulanier, G., Török, T., Démoulin, P., & DeLuca, E. E. 2010, *ApJ*, 708, 314
- Botha, G. J. J., Arber, T. D., & Srivastava, A. K. 2012, *ApJ*, 745, 53
- Brown, D. S., Nightingale, R. W., Alexander, D., et al. 2003, *Sol. Phys.*, 216, 79
- Del Zanna, G., Tripathi, D., & Young, P. 2011, *Astronomy and Geophysics*, 52, 020000
- Fan, Y., & Gibson, S. E. 2004, *ApJ*, 609, 1123
- Foullon, C., Verwichte, E., Nakariakov, V. M., Nykyri, K., & Farrugia, C. J. 2011, *ApJ*, 729, L8
- Freidberg, J. P. 1982, *Reviews of Modern Physics*, 54, 801
- Gibson, S. E., & Fan, Y. 2006, *ApJ*, 637, L65
- Gilbert, H. R., Holzer, T. E., Burkepile, J. T., & Hundhausen, A. J. 2000, *ApJ*, 537, 503
- Goldston R. J. & Rutherford, P. H. 1995, *Introduction to Plasma Physics*
- Haynes, M., & Arber, T. D. 2007, *A&A*, 467, 327
- Hillier, A., Isobe, H., Shibata, K., & Berger, T. 2012, *ApJ*, 756, 110
- Hillier, A., Berger, T., Isobe, H., & Shibata, K. 2012, *ApJ*, 746, 120
- Hood, A. W., & Priest, E. R. 1979, *Sol. Phys.*, 64, 303
- Innes, D. E., Cameron, R. H., Fletcher, L., Inhester, B., & Solanki, S. K. 2012, arXiv:1202.4981
- Kadomtsev, B. B. 1966, *Reviews of Plasma Physics*, 2, 153
- Kliem, B., Karlický, M., & Benz, A. O. 2000, *A&A*, 360, 715
- Kumar, P., Srivastava, A. K., Somov, B. V., et al. 2010, *ApJ*, 723, 1651
- Kumar, P., Cho, K.-S., Bong, S.-C., Park, S.-H., & Kim, Y. H. 2012, *ApJ*, 746, 67
- Leka, K. D., Fan, Y., & Barnes, G. 2005, *ApJ*, 626, 1091
- Lemen, J. R., Title, A. M., Akin, D. J., et al. 2012, *Sol. Phys.*, 275, 17
- Liu, R., Alexander, D., & Gilbert, H. R. 2007, *ApJ*, 661, 1260
- Ofman, L., & Thompson, B. J. 2011, *ApJ*, 734, L11
- O'Dwyer, B., Del Zanna, G., Mason, H. E., et al. 2011, *A&A*, 525, A137
- Priest, E. R. 1982, *Dordrecht, Holland ; Boston : D. Reidel Pub. Co. ; Hingham,*, 74P
- Sakai, J.-I., & de Jager, C. 1996, *Space Sci. Rev.*, 77, 1

- Soler, R., Arregui, I., Oliver, R., & Ballester, J. L. 2010, *ApJ*, 722, 1778
- Srivastava, A. K., Zaqarashvili, T. V., Kumar, P., & Khodachenko, M. L. 2010, *ApJ*, 715, 292
- Sturrock, P. A. 1994, *Plasma Physics, An Introduction to the Theory of Astrophysical, Geophysical and Laboratory Plasmas*, ISBN 0521448107, Cambridge University Press, 1994.
- Shibasaki, K. 1999, *Proceedings of the Nobeyama Symposium*, 419
- Syrovatskii, S.I., 1981, *Ann. Rev. Astron. Astrophys.*, 19, 163
- Tajima, T., Brunel, F., & Sakai, J. 1982, *ApJ*, 258, L45
- Taroyan, Y. 2011, *A&A*, 533, A68
- Taroyan, Y., & Ruderman, M. S. 2011, *Space Sci. Rev.*, 158, 505
- Török, T., & Kliem, B. 2005, *ApJ*, 630, L97
- Török, T., Kliem, B., & Titov, V. S. 2004, *A&A*, 413, L27
- Tripathi, D., Gibson, S. E., Qiu, J., et al. 2009, *A&A*, 498, 295
- Tripathi, D., Solanki, S. K., Mason, H. E., & Webb, D. F. 2007, *A&A*, 472, 633
- Tripathi, D., Gibson, S. E., Joshi, N.C., Srivastava, A.K., *ApJ*, 2013, in preparation
- Tsap, Y. T., Kopylova, Y. G., Stepanov, A. V., Melnikov, V. F., & Shibasaki, K. 2008, *Sol. Phys.*, 253, 161
- Williams, D. R., Török, T., Démoulin, P., van Driel-Gesztelyi, L., & Kliem, B. 2005, *ApJ*, 628, L163
- Yan, X. L., & Qu, Z. Q. 2007, *A&A*, 468, 1083
- Zaqarashvili, T. V., Díaz, A. J., Oliver, R., & Ballester, J. L. 2010, *A&A*, 516, A84

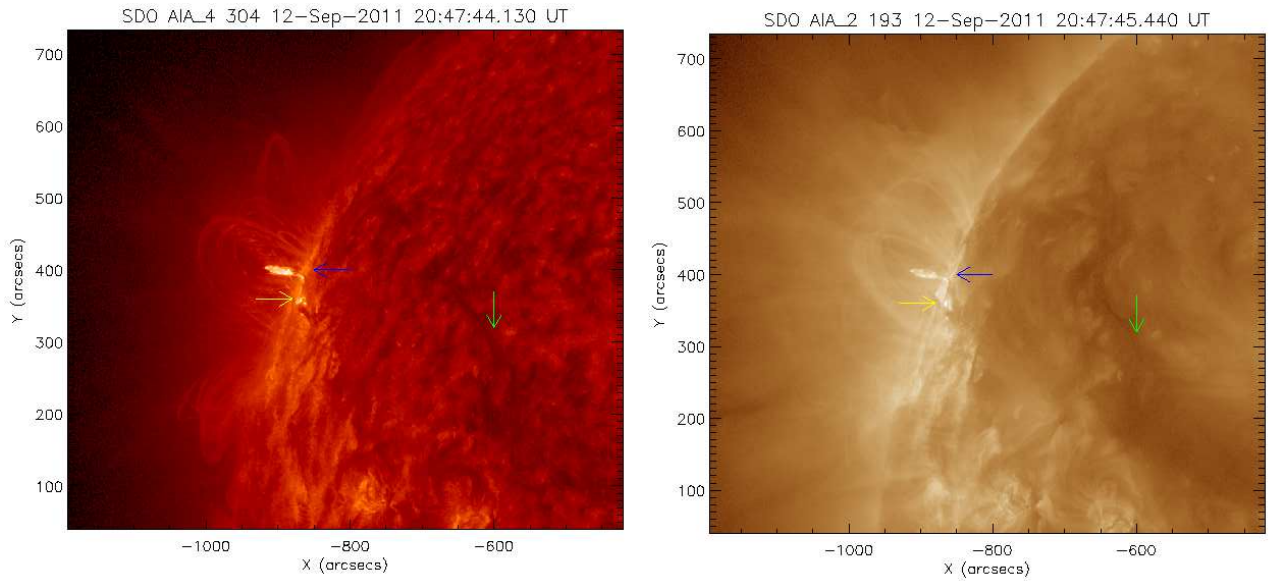


Fig. 1.— SDO/AIA 193 Å (right) and 304 Å (left) EUV images showing the filament channel (green-arrow), activated filamentary part (yellow-arrow), rising instable flux-rope and overlying loops (blue-arrow) in AR11295 well before the flare.

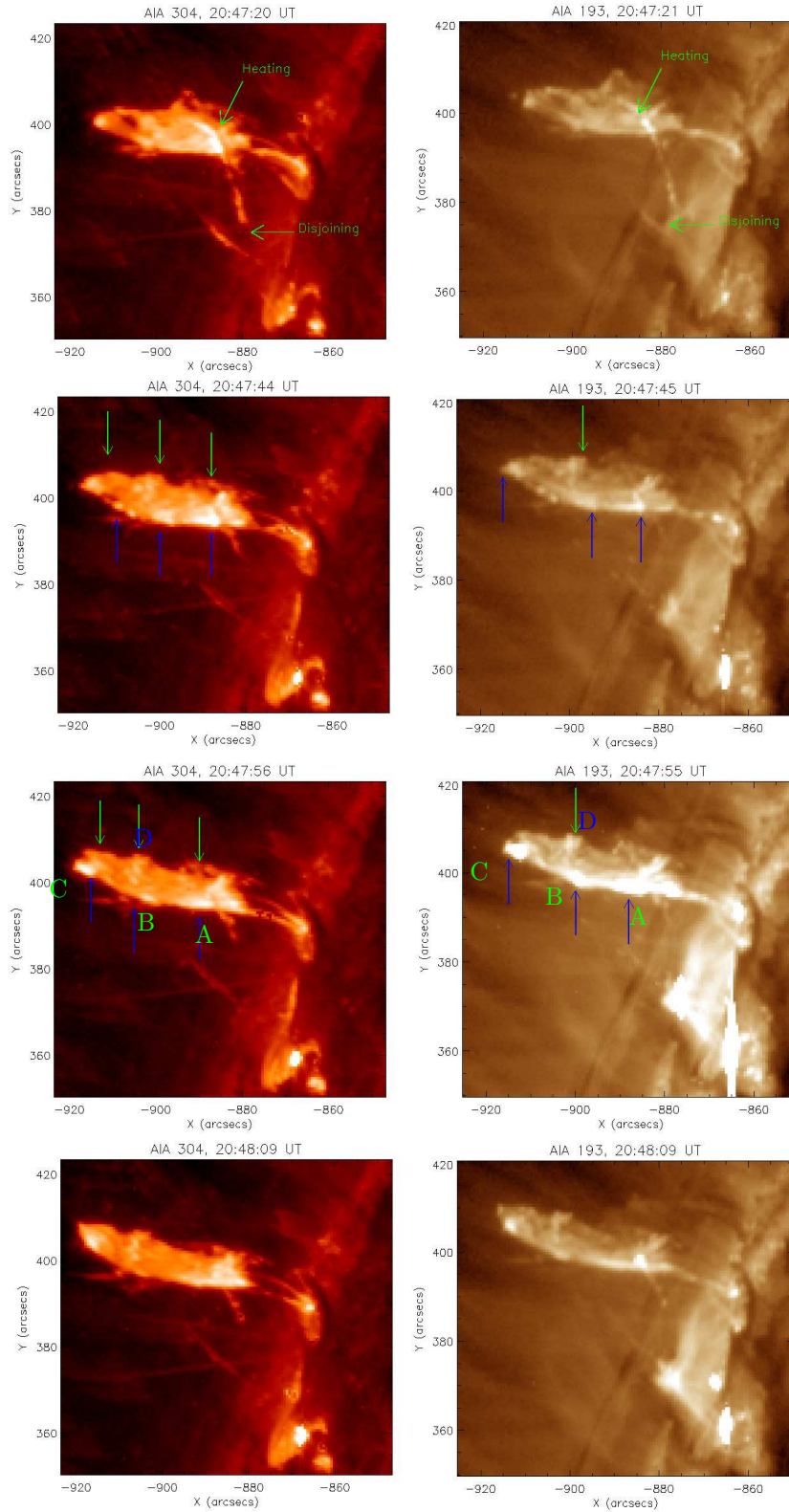


Fig. 2.— SDO/AIA 304 Å and 193 Å temporal image data showing the evolution of sausage-pinch instability. The formation of enhanced density as well as increased cross-sections are clearly evident over the fluxtube, which is overlying the complex active region. The three blue arrows on 193 Å (20:47:55 UT) and 304 Å (20:47:57 UT) snapshots respectively mark (right to left) the positions 'A', 'B', and 'C', while the green arrow marks the position 'D', where surface curvatures are evolved and rippled out.

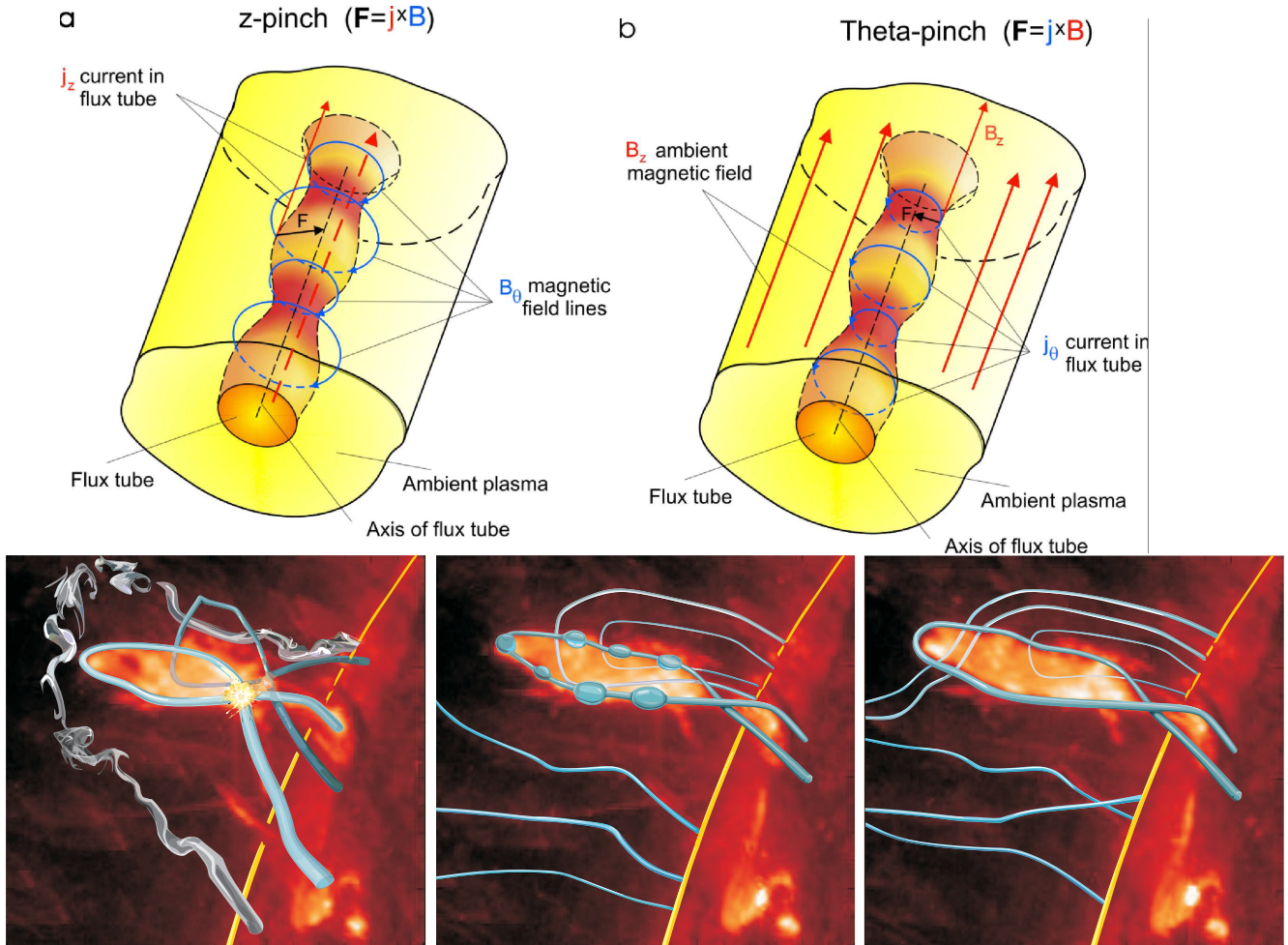


Fig. 3.— Top-panel : Sketch of the physical mechanism of sausage instability in z -pinch (a) and θ -pinch (b). In the case (a), when an $m = 0$, i.e. sausage perturbation is superimposed on the flux tube, the magnetic field, B_θ , (shown as blue cylindrical arrows) in the neck region grows due to the current j_z (shown as dashed red arrow inside the magnetic flux tube) increasing in a smaller cross section. Additional magnetic pressure produces a force (F) which tends to constrict the plasma cylinder. Bottom-panel : The handmade sketches overlaid on AIA 304 Å snapshots to explain the observed scenario. The observed localized dynamics of the fluxtube is generated by either of these two physical mechanisms, i.e., θ or z -pinch.

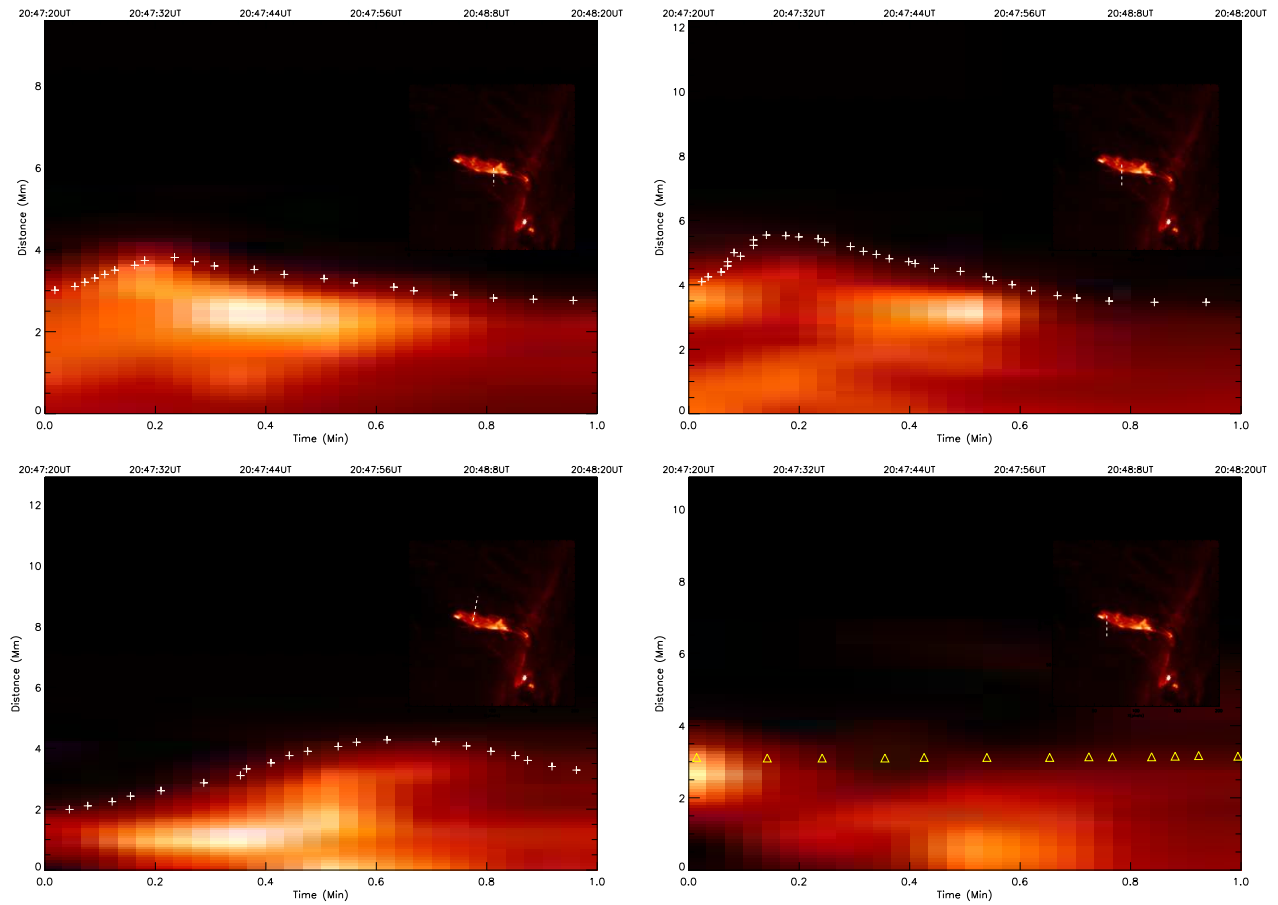


Fig. 4.— Distance-Time diagrams in AIA 304 Å along the slits drawn across the various surface curvatures over the flux tube marked by position 'A', 'B' (on southward part), 'D' (on northward part). Last panel shows almost none variation of the surface of clearly evolved narrow neck between knot B and C (Fig. 2).

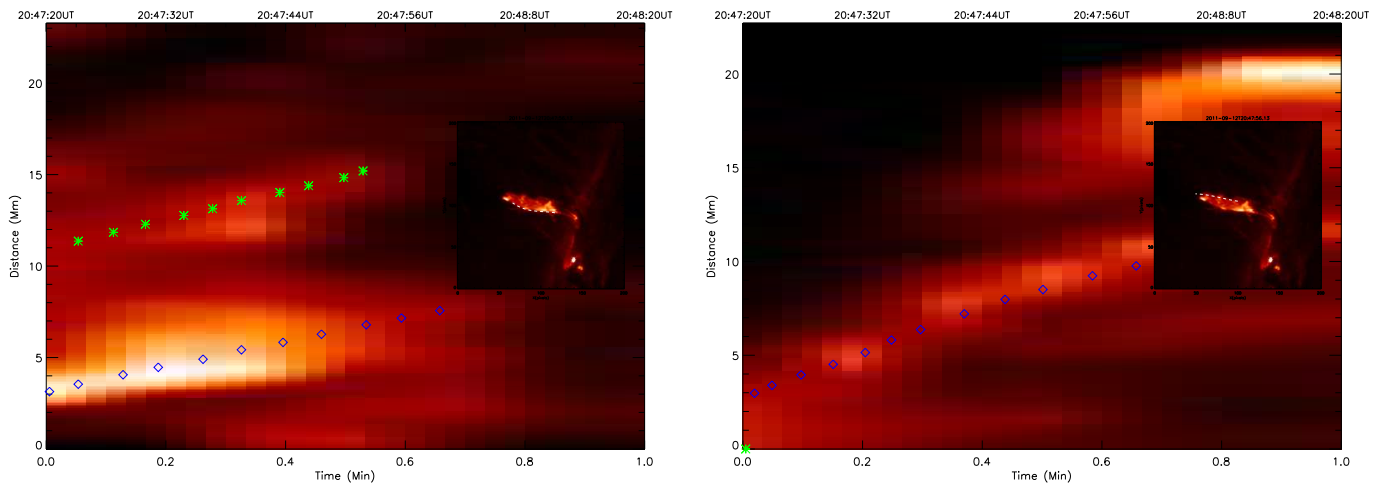


Fig. 5.— Distance-Time diagram in AIA 304 Å along the curved path drawn along the southward part of the enveloping flux tube that shows the plasma (brightness) motion through two knots as marked by position 'A' (diamonds) and 'B' (stars), as well as on its northward part that consists the dynamic and bright knot 'D' (cf., motion of brightness as marked by diamond symbols) in Fig. 2.